Chapter 4

Acoustic Emission Application for Monitoring Bearing Defects

Zahari Taha and Indro Pranoto

Additional information is available at the end of the chapter

http://dx.doi.org/10.5772/55434

1. Introduction

Several studies have been conducted to investigate AE application in bearing defects diagnosis and monitoring. The application of AE to measure the condition of slow speed antifriction bearings on off-shore gas production platform slewing cranes have been investigated by Rogers [1]. It was found that AE sensors can detect defects before they appeared in the vibration acceleration range and can also detect possible sources of AE generated during a fatigue life test of thrust loaded ball bearing [2, 3]. Morhain and David [4] showed the application of AE to monitor defects on the inner and outer races of split bearings.

Some researchers have studied AE based on the types of defects, locations, and various bearing operation condition. Smith and Fadden [5,6] identified the acoustic emission signals to detect defects in the form of a fine scratch on the inner race of axially loaded angular contact ball bearing at low speed only. The usefulness of some acoustic emission parameters, such as peak amplitude and count for detection of defects in radially loaded ball bearings at low and normal speed have been demonstrated [7].

Tan [8] suggested that, measurement of the area under the amplitude-time curve is a preferred method for detection of defects in rolling element bearings. Distribution of events by counts and peak amplitude has been used for detecting bearing defects [9]. Hawman and Galinaitis [10] noted that diagnosis of bearings defect is accomplished by high-frequency modulation of AE bursts at the outer race frequency.

The types of bearing used will affect the types of defects criteria to be simulated. Some researchers have used many types of bearings. Choudury and Tandon [11] have used the NJ series cylindrical roller bearing of normal clearance with five sizes of SKF bearing. NJ series bearings were chosen because the inner races of these bearings can be easily separated and thus the creation of simulated defects on the inner races and the rollers become easier. One

simulated defect was introduced across the length of a roller bearing and the inner raceway by spark erosion technique. Cooper split-type roller bearing was selected with assembly and disassembly accomplished with minimum disruption to the test sequence. Two defect types used were surface discontinuity of the outer race and material protrusions that are clearly above the average surface roughness [12]. C.J Li and S.Y Li [13] used the ball bearing under four conditions: good bearing, a bearing with a groove on its outer race, bearing with a single roller defect, and a bearing with three outer race defects. The size of the artificial defects was 15.2 mm in diameter by 0.127 mm in depth and the width of the groove was 2 mm.

Choudury and Tandon [11] used the counts and statistical distribution of events by counts and peak amplitudes, and showed that as the defect size increases, more events are emitted with higher values of peak amplitudes and counts. It was also shown that the increase in counts is much greater than in other parameters, such us events and peak amplitudes. C.J Li and S.Y Li [13] showed that defects at different location of bearing (inner race, roller, and outer race) will have characteristic frequencies at which bursts are generated. The signal emitted by damaged bearing consists of periodic bursts of AE. The signal is considered to be amplitude modulated at the characteristic defect frequency.

Traditional techniques were used for detecting localized defects mainly based upon the processing of vibration and sound measured near the bearing with time domain techniques such as: peak level and r.m.s value [14], crest factor analysis [15], kurtosis analysis [16], and shock pulse counting [17]. Counts, events, and peak amplitude of the signal can be investigated and compared with each other to find more sensitive and accurate values.

In roller bearing application, the forces transmitted in the bearing give rise to stresses of varying magnitudes between the surfaces in both rolling and sliding motion. As a result of repeated loads concentrated contacts, changes occur in the contact surfaces and in the regions below the surfaces. These changes cause surface deterioration or wear [18]. The loss or displacement of material from the surface will cause wear. Material loss may be loose debris.

Mild mechanical wear
Adhesive wear
Smearing
Corrosive (tribochemical) wear
Plastic flow
Surface indentation
Abrasive wear
Surface distress
Pitting
Fatigue spalling

Table 1. Bearing Failure Classification Due to Wear [18]

http://dx.doi.org/10.5772/55434

Material displacement may occur by local plastic deformation or the transfer of material from one location to another location. When wear has reached the level that it threatens the essential function of the bearing, the bearing is considered to have failed. Bearing failures can be classified as in table 1.

In this research AE data is analyzed in the time domain. Peak amplitude, r.m.s., and AE counts were investigated and correlated with the type of defects, size of defect, speed, and applied load.

2. Experimental setup

A sketch of the rig on which the experiments were conducted is shown in figure 1. It consists of a shaft (2) supported on the base plate of a lathe machine and mounted on the chuck mounting. The bearing housing (5) supports the test bearing and is mounted on a base plate. The bearing housing is a plummer block housing type, SKF-SNL 516-513 series. Bolts, nuts, and washers are used to mount it on the base plate. Locating rings inside the housing restrict the movement of the shaft.

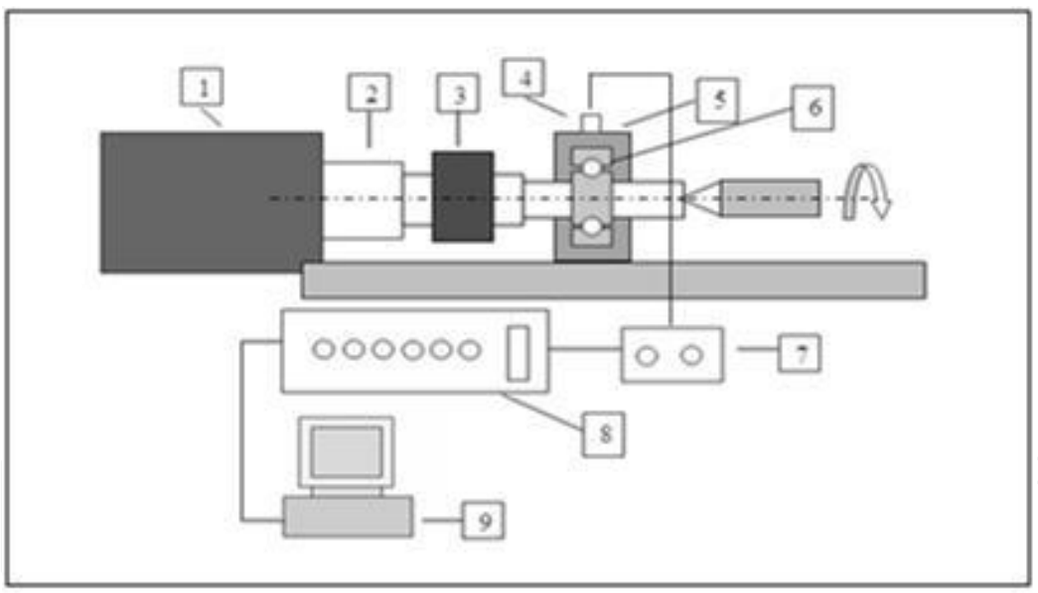

1. Motor driver, from spindle of Colchester lathe machine
2. Shaft
3. Load
4. AE sensor
5. Bearing housing
6. Test bearing
7. Piezotron AE Coupler
8. Signal Conditioning
9. PCI Data Acquisition (DAQ)

Figure 1. The experimental setup diagram

The shaft is extended beyond the right tailstock of the lathe machine such that the test bearing (6) may be easily mounted or dismounted from it. The extended portion of the shaft is stepped and of varying diameter to allow testing of different sizes of bearings and also to vary the load. The drive to test the rig is provided by the spindle of the lathe machine (1) and transmitted through a chuck mounted on the shaft. The speed of the rig can be adjusted easily by a variable control speed knob between the ranges 0 up to 3,250 rpm. To apply radial load on the test bearing a pulley load model is used (3). The pulley load is designed and calibrated to satisfy the load testing condition. The AE sensor (4) is mounted on the top of the test bearing housing by a magnetic clamp so that the measurement is performed in the nearest zone of the burst signal.

3. Test bearings and housing

The test bearings used in the study are self-aligning ball bearings from SKF series 1311 ETN9 with inside bore diameter 55 mm, outside diameter 120mm, and width 29 mm (figure 2). These bearings can self-align while operating inside the housing and also the inner race can be easily separated thus the creation of simulated defects on the inner races and rollers become easier.

The test bearing has a double row, consisting of 30 ball elements with 15 balls in each row. The bearing has dynamic and static load rating of 50.7 KN and 18 KN, respectively, a maximum speed rating of 7500 rpm, and weighs 1.6 kg. The appropriate bearing housing for the self-aligning ball bearing series 1311 ETN9 is the SNL 513-611 plummer block housing type from SKF. The housing encapsulates the test bearing and provide space for mounting the AE sensor. Figures 2 to 5 show the experimental set-up of the test bearings.

Figure 2. SKF Self aligning ball bearing used as test bearing

http://dx.doi.org/10.5772/55434

Figure 3. Test bearing arrangement on the housing, locating rings, and others equipments

Figure 4. Shaft, test bearing, and the housing arrangement on the lathe machine

Figure 5. A view of the experimental set-up

4. Instrumentation

Measurements were carried out using an instrumentation system that consist of an AE sensor Kistler 8152 B121, an AE PZT coupler Kistler 5125B2, a DAQ card NI 6034 E, a BNC connector NI, signal conditioning SC 2345 NI, and Lab view software on a PCI system (Figures 6 to 8). The AE sensor has a frequency range of 50 – 400 kHz, 10 dB, sensitivity 57 dBref 1V/(m/s) and is mounted on the test bearing using a magnetic clamp from Kistler.

An AE PZT coupler with a gain process the high frequency output signals from the sensor and filter the signals. The gain can be set with a jumper. The frequency output of the coupler has an AE RMS output in a range of 10-1000 kHz and AE filtered output of 5-1700 kHz. The data acquisition NI 6034E series have 16 analog inputs at up to 200 kS/s, 16-bit resolution and Lab View 7.0 software is used for acquiring and processing the data. The AE PZT coupler is powered by a DC power supply with 0-2 A current range and 0-30 V voltage range.

5. AE sensor

In this research, the AE signal is obtained from an AE sensor. The sensor used is a Kistler AE sensor type 8152 B121. The sensor has an integral impedance converter for measuring AE above 50 kHz. With its small size it mounts easily near the source of emission to optimally capture the signal. The sensor has a very rugged welded housing (with degree of protection IP 65 PUR or IP 67 Viton).

The AE sensor consists of the sensor housing, the piezoelectric sensing element, and the built-in impedance converter. The sensing element is made of piezoelectric ceramic and mounted on a thin steel diaphragm. Its construction determines the sensitivity and frequency response of the sensor. The sensor have the capability of high sensitivity and wide frequency range, inherent high-pass-characteristic, insensitive to electric and magnetic noise field, and ground isolated to prevents ground loops. The sensor is mounted in the bearing housing with a magnetic clamp (figure 6)

Figure 6. AE sensor mounting on the bearing housing with a magnetic clamp

http://dx.doi.org/10.5772/55434

Figure 7. Instrumentation apparatus: PCI DAQ card, Connector block, and DC power supply

Figure 8. Data acquisition board signal conditioning SC-2345

6. AE–Piezotron coupler

The AE-Piezotron Coupler processes the high frequency output signal from AE sensor (Figure 9). Gain, filters, and integration time constant of the built-in-RMS converter are design as plug-in modules. This allows the best possible adaptation to the particular monitoring function. The gain can be set until 100 times. The amplifier has two series-connected second order filters, design as plug elements. The types of filter (high pass or low-pass) as well as the frequency limit are freely selectable.

A band pass filter is obtained by the series connection of one high-pass and one low-pass filter. The integration time constant of the RMS converter can also be freely selected. The limit switch is set with a potentiometer, and the switching threshold set point can be monitored at the limit output with an oscilloscope. The output of the limit switch is electrically isolated by an optocoupler. The output signals are available at the 8-pole round connector: two analog output signals AE output (Filter), AE-Out (RMS) and a Digital output signal (Limit Switch)

Figure 9. AE Piezotron Coupler Data Acquisition and Processing

6.1. PCI data acquisition board 6034E

Data acquisition system is implemented by a PCI 6034 E card. Data acquisition is performed using the Lab View 7.0 software and NI-DAQ Driver. The NI- DAQ has an extensive library of functions that can be called from an application programming environment. In this research, buffered data acquisition function is used as high speed A/D conversion process.

The NI-DAQ also has a high-level DAQ-I/O function for maximum capacity. The example of high-level function is streaming data to the hard disk or acquiring a certain number of data points. NI-DAQ maintains consistent software interface among its different version so that the platform can be changed with minimal modification to the software code.

In data acquisition application, there are many programs language that can be used. Zang illustrated the application of data acquisition developed using the NI-DAQ driver software and also show the relationship with other software and environment (Figure 10) [19].

6.2. Data acquisition and user interface

In this research, when monitoring the bearing defects, AE signal was captured using the Lab View Library. The data obtained was sampled using the windows XP interface to display the correlation graph and trend of AE signal. The Lab View 7 Software provides the Windows interface that makes the data processing more user friendly. Figure 11 describes the process of data acquisition and processing in this research.

7. AE counts and threshold level

The AE counts indicates the number of times the amplitude exceeds a preset voltage in a given times and gives a simple number characteristic of the signal. Many researchers have investigated the used of AE counts to detect defects on the bearing. Mba and Rao [9] stated that the successful use of AE counts for bearing diagnosis is dependent on the particular investigation, and the method of determining the trigger level is at the discretion of the investigator. They also stated that AE counts are also sensitive to the level and grade of lubricant within the bearing, adding the complexity of this measure.

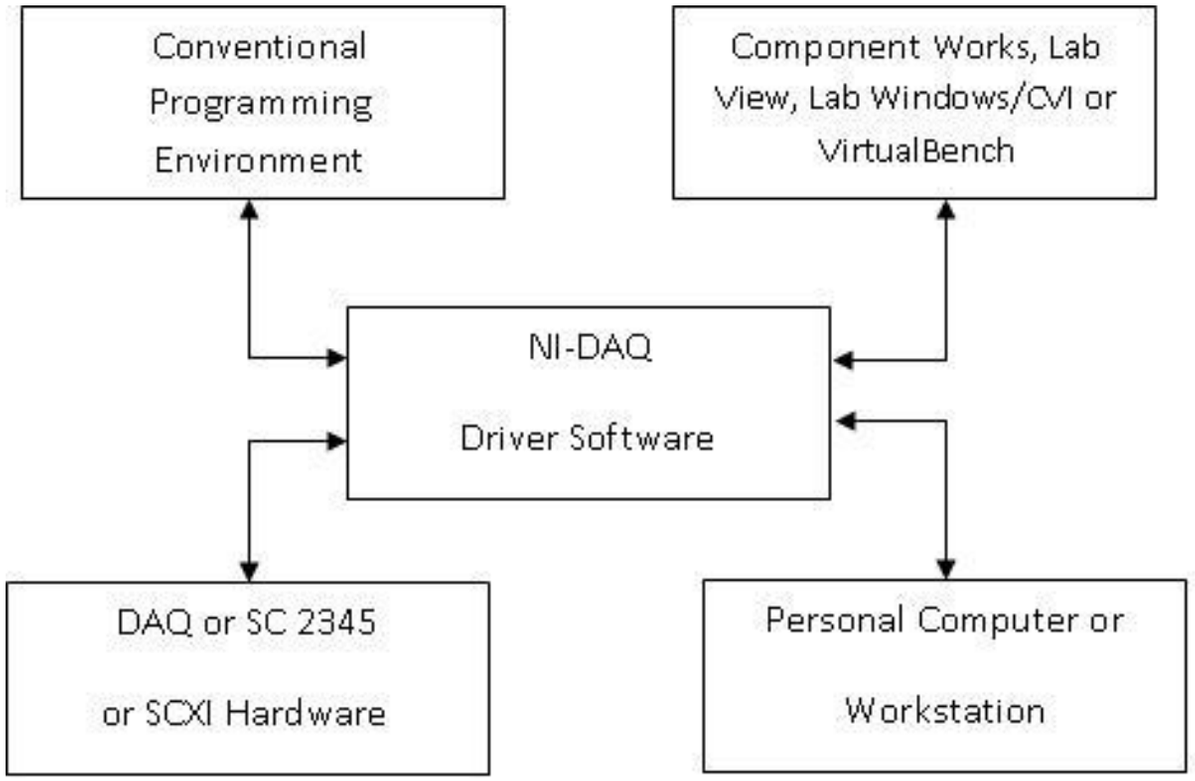

Programming Environment [19]

Figure 10. Relationship between the NI-DAQ Software and Hardware

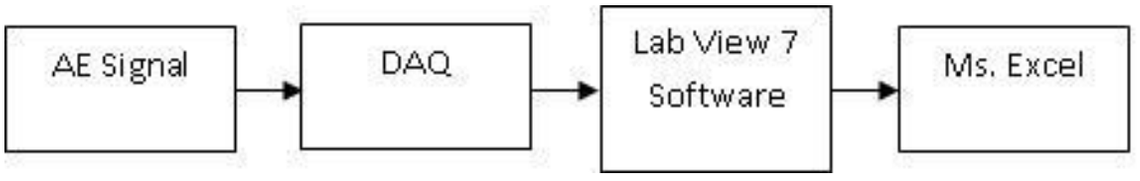

Figure 11. The schematic diagram of acquisition and processing the data

Morhain and Mba undertook an investigation to ascertain the most appropriate threshold level for AE counts diagnosis in rolling element bearings. The result shows that values of AE maximum amplitude did correlate with increasing speed but not with load and defect size. In addition, they stated that the relationship between bearing mechanical integrity and AE counts is independent of the chosen threshold level, although a threshold of at least 30% of the maximum amplitude for the lowest speed and load operating condition was suggested [4].

To calculate the AE counts from the defects, there are some parameters that have to be determined:

1. Maximum amplitude of background noise
2. The preset or threshold level as a reference to calculate the number of times the AE of defects exceed it.

The data processed from Lab View and Ms Excel gives the maximum amplitude of background noise and the defects. The characteristic of a maximum amplitude of AE is a burst signal, which is the maximum amplitude in the time domain graph that is not frequently distributed. Using the maximum amplitude as a reference of AE counts is not recommended.

Investigation of preset values in wide ranges of percentages of maximum amplitudes of background noise is useful to calculate the AE counts. The percentage levels of maximum amplitude are called threshold levels. The threshold levels ensure that the AE counts are calculated in wide ranges percentages of maximum amplitude of AE. Investigation of the AE counts in many threshold levels is useful to get the appropriate threshold levels range in real time monitoring.

In this study, the threshold levels were chosen as percentage of maximum amplitude of the corresponding background noise level. For example to calculate the AE counts for ball defect at 1500 rpm, the threshold level will be the percentage of the maximum amplitude of background noise at 1500 rpm (N15L0). In order to investigate the relationship between the threshold level and AE counts, five threshold values were calculated at varying percentages. The percentage values selected were 10%, 30%, 50%, 70%, and 90%. The wide ranges of values will be useful for determining the influence of threshold value on AE count result. The threshold levels for all rotational speed are show in table 2 below:

Threshold Value						
Noise Condition	**Maximum Voltage (volt)**	**Amplitude Level (volt) for Each Percentage**				
		10%	30%	50%	70%	90%
N3L0	0.6	0.06	0.18	0.30	0.42	0.54
N5L0	1.2	0.12	0.36	0.60	0.84	1.08
N7L0	1.8	0.18	0.54	0.90	1.26	1.62
N15L0	6.3	0.63	1.89	3.15	4.41	5.67
N30L0	18.15	1.82	5.45	9.08	12.71	16.34

Table 2. Threshold value for different noise condition

8. AE counts of ball defects

The number of AE counts for ball defect size 1 is shown in figures 12 to 16 below. Figures 17 to 21 show the number of AE counts for ball defect size 2.

http://dx.doi.org/10.5772/55434

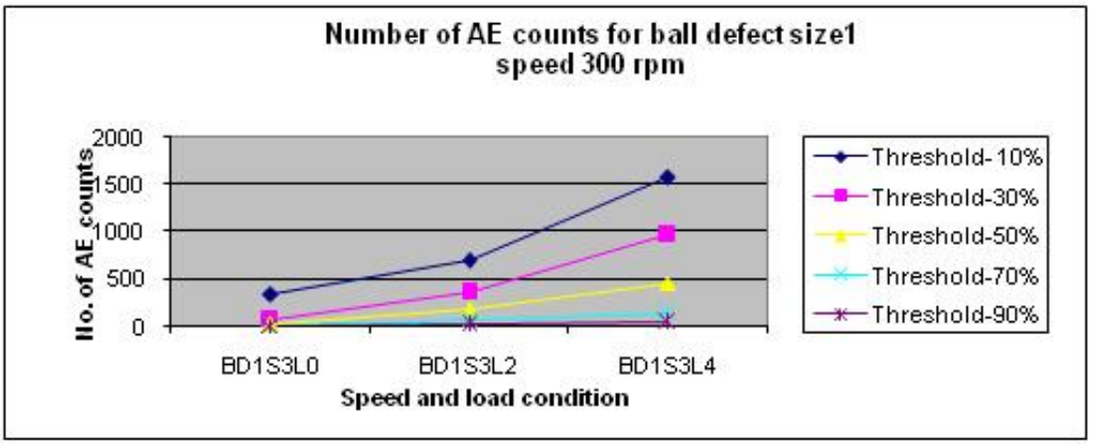

Figure 12. Number of AE counts for ball defect size 1 at speed 300 rpm

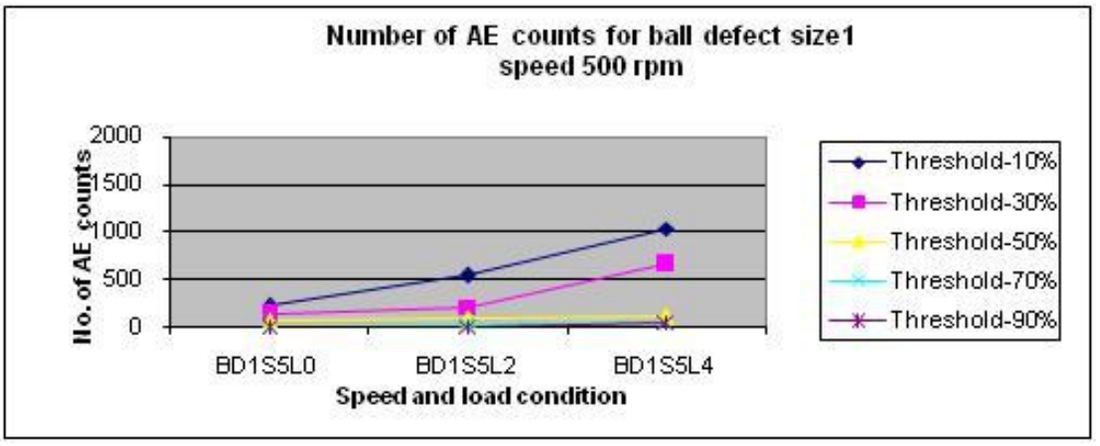

Figure 13. Number of AE counts for ball defect size 1 at speed 500 rpm

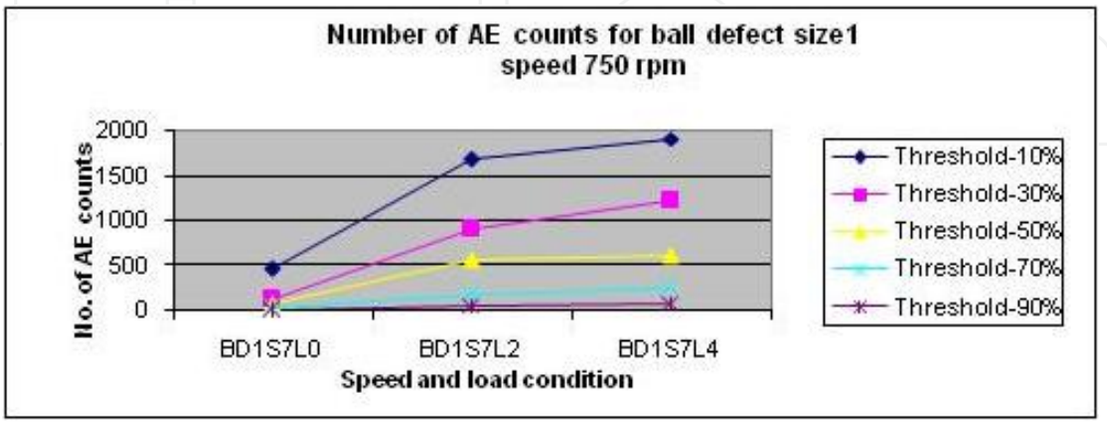

Figure 14. Number of AE counts for ball defect size 1 at speed 750 rpm

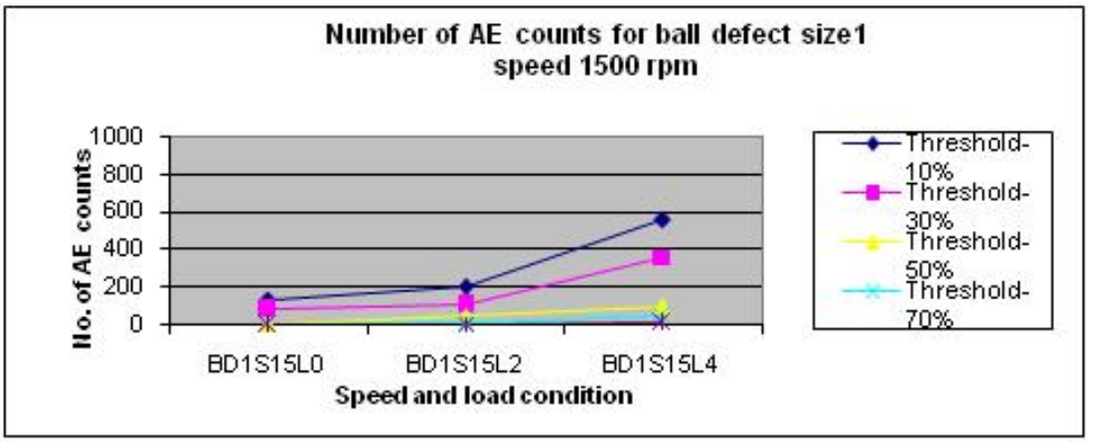

Figure 15. Number of AE counts for ball defect size 1 at speed 1500 rpm

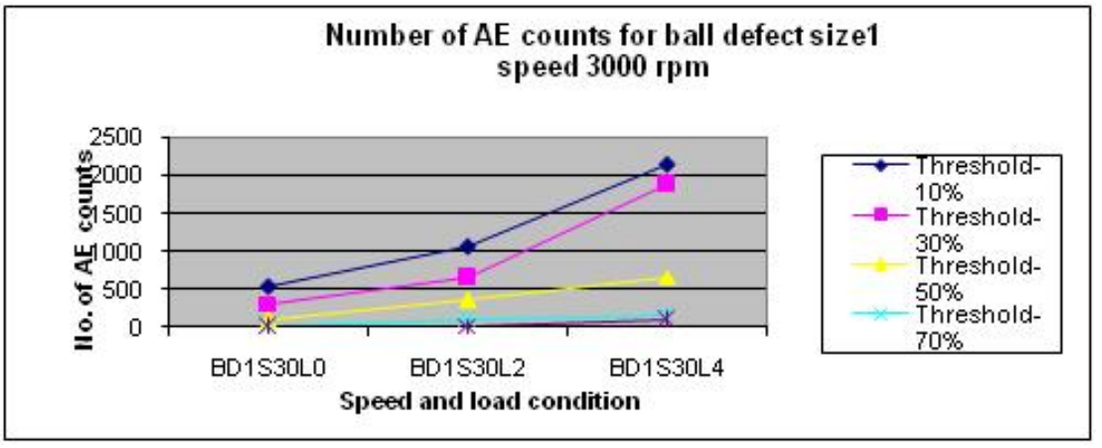

Figure 16. Number of AE counts for ball defect size 1 at speed 3000 rpm

From the result of AE counts in ball defect size 1, the value of AE counts increases with increasing load for all level of threshold. The increasing value is seen more clearly at percentages 50%, 30%, and 10%. This phenomenon is also observed from the result of AE counts in ball defect size 2, as shown in figures 17 to 21 below. The results also show that the number of AE counts of ball defect size 2 is greater than counts of size 1 for each respective rotational speed level and load. The graph for ball defect size 2 also indicates that, at percentages level of 50%, 30%, and 10% the AE counts clearly increases as the load increases.

In ball defect analysis, the result clearly showed that the AE counts increases with increasing load and size of defect at all rotational speed. The results are very clear at threshold level at or less than 50 % (50%, 30%, and 10%).

http://dx.doi.org/10.5772/55434

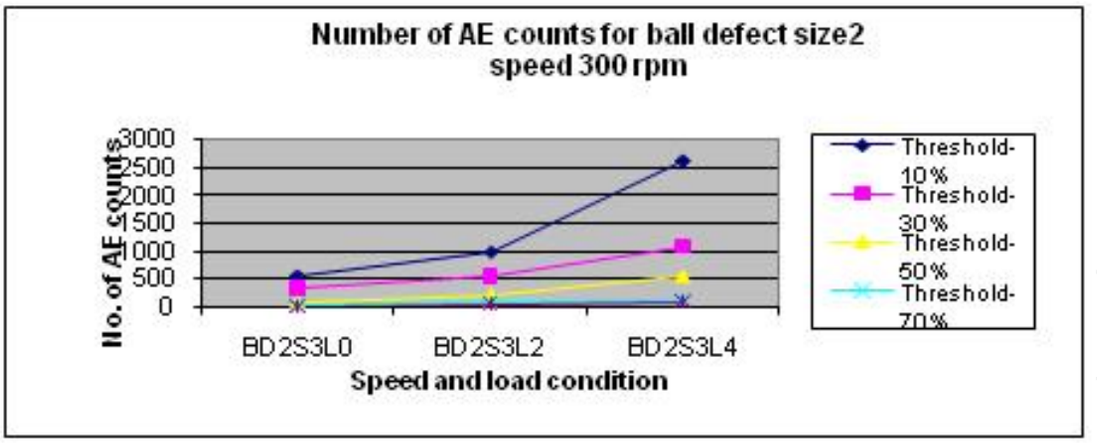

Figure 17. Number of AE counts for ball defect size 2 at speed 300 rpm

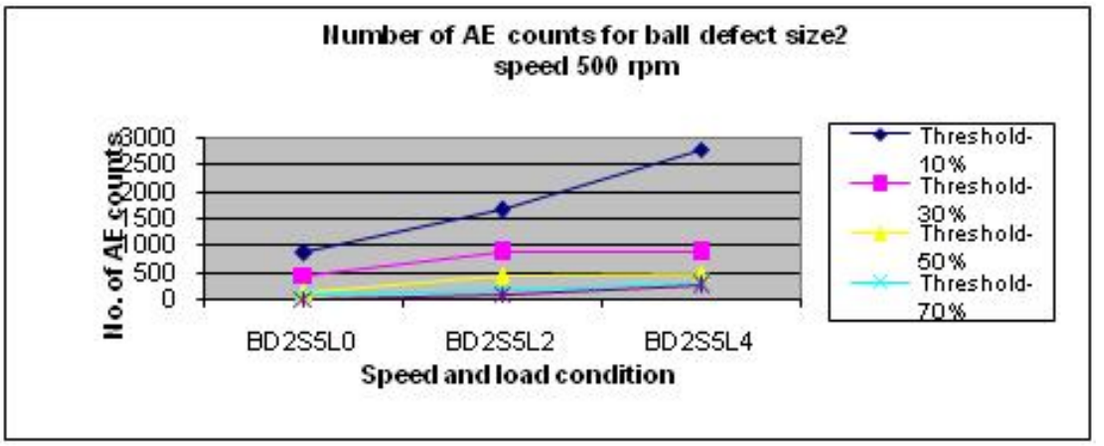

Figure 18. Number of AE counts for ball defect size 2 at speed 500 rpm

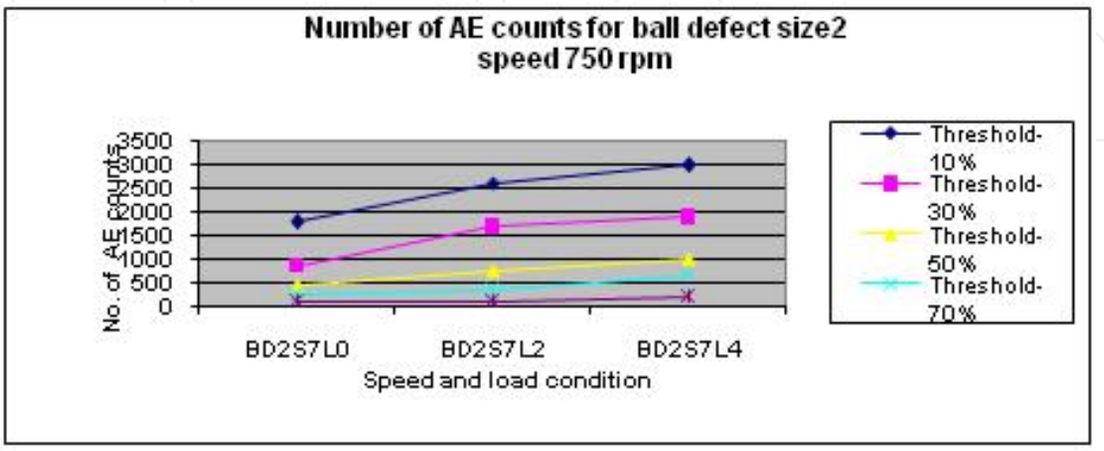

Figure 19. Number of AE counts for ball defect size 2 at speed 750 rpm

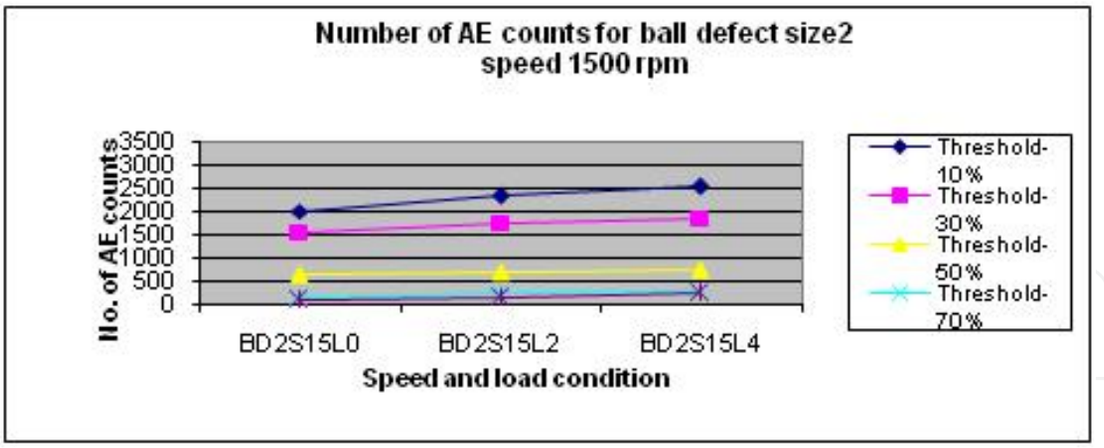

Figure 20. Number of AE counts for ball defect size 2 at speed 1500 rpm

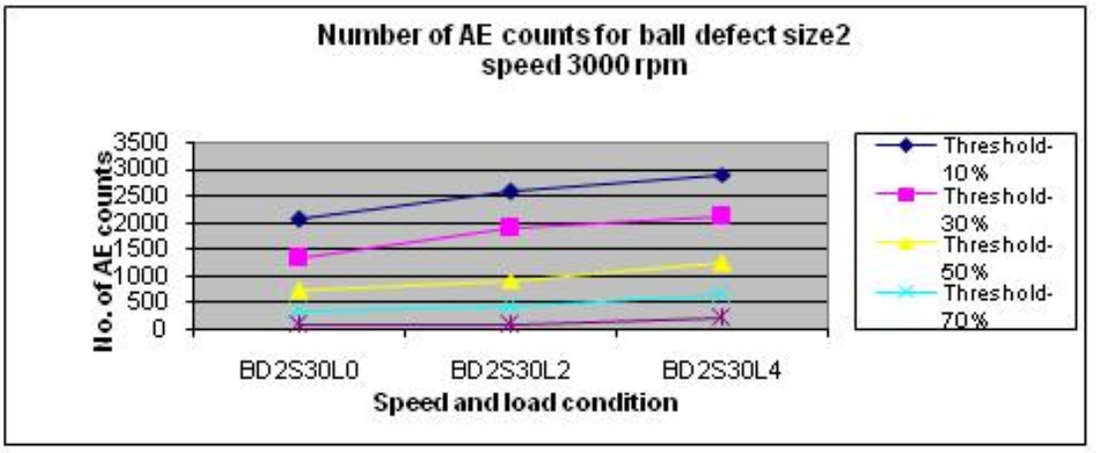

Figure 21. Number of AE counts for ball defect size 2 at speed 3000 rpm

9. AE counts of inner race defects

The number of AE counts for inner race defect size 1 are shown in figures 22 to 26 below and figures 27 to 31 show the number of AE counts for inner race defect size 2.

The result of AE counts in the inner race defect shows different phenomenon compared with the ball defect. For the inner race defect size 1, at 300 rpm and 500 rpm the AE counts increases as the load increases at threshold levels of 30% and 10%. Whilst at 750 rpm, 1500 rpm, and 3000 rpm the AE counts increases as load increases at 50%, 30%, and 10% threshold levels. In general the AE counts increases with increasing load.

http://dx.doi.org/10.5772/55434

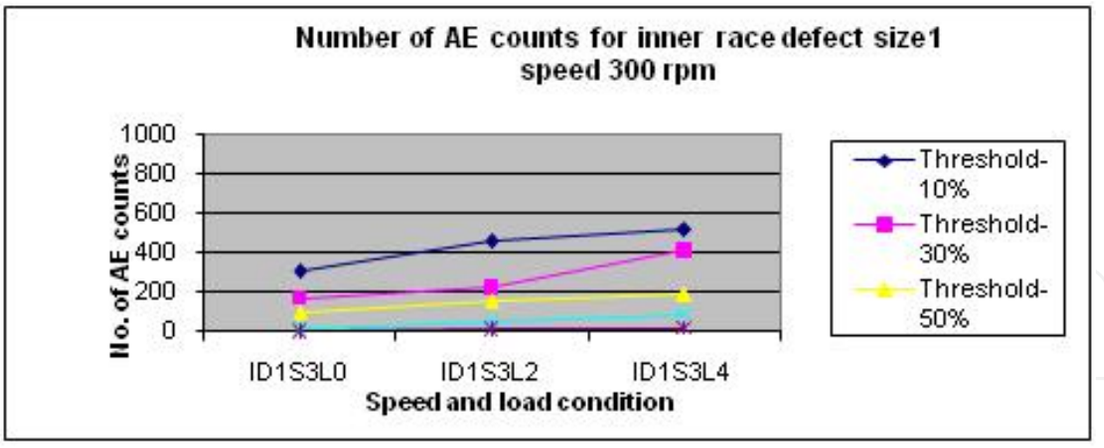

Figure 22. Number of AE counts for inner race defect size1 at speed 300 rpm

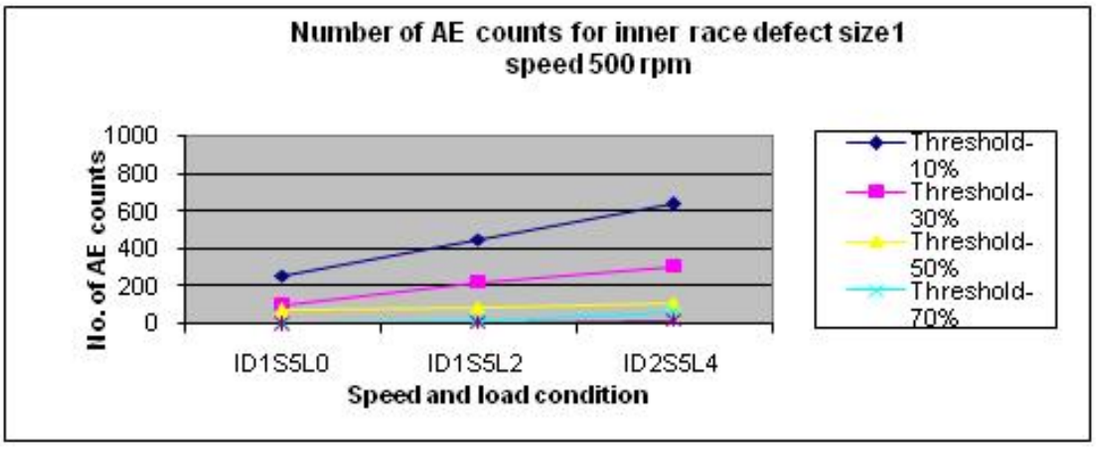

Figure 23. Number of AE counts for inner race defect size 1 at speed 500 rpm

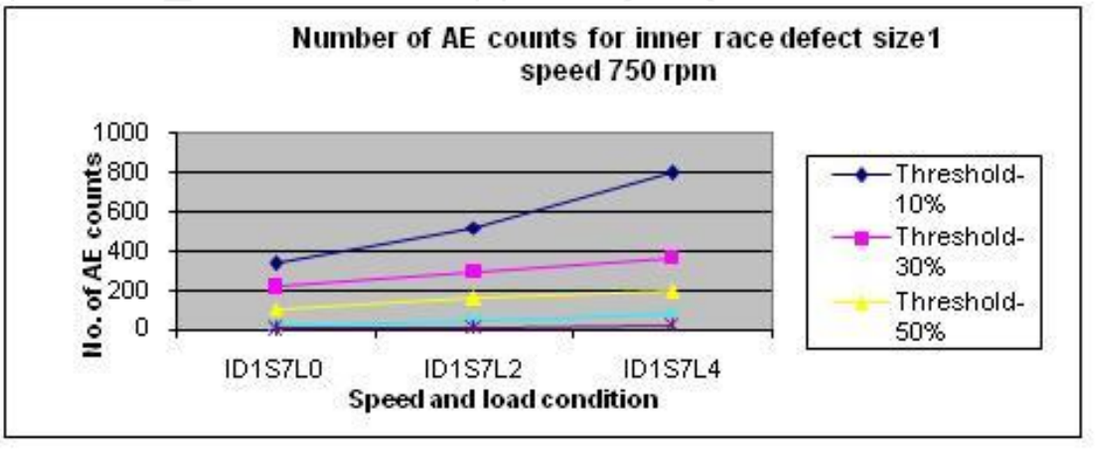

Figure 24. Number of AE counts for inner race defect size1 at speed 750 rpm

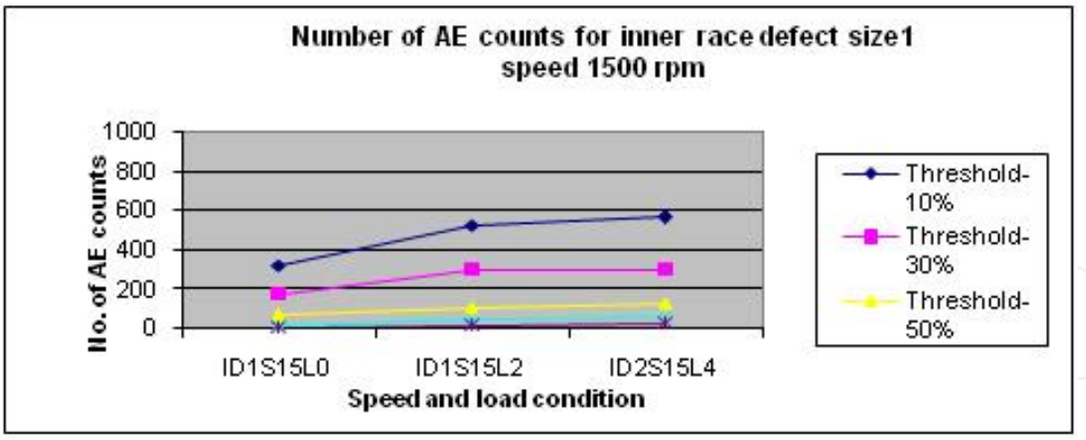

Figure 25. Number of AE counts for inner race defect size1 at speed 1500 rpm

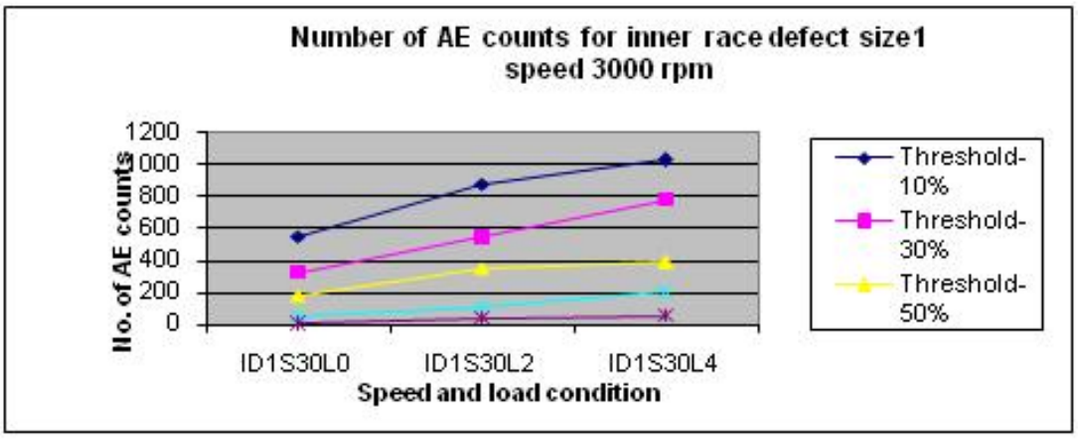

Figure 26. Number of AE counts for inner race defect size1 at speed 3000 rpm

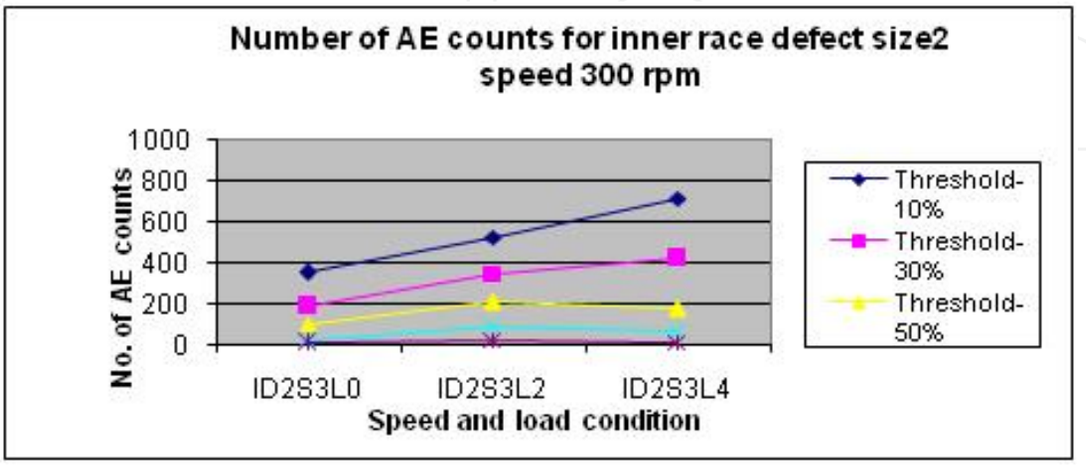

Figure 27. Number of AE counts for inner race defect size2 at speed 300 rpm

http://dx.doi.org/10.5772/55434

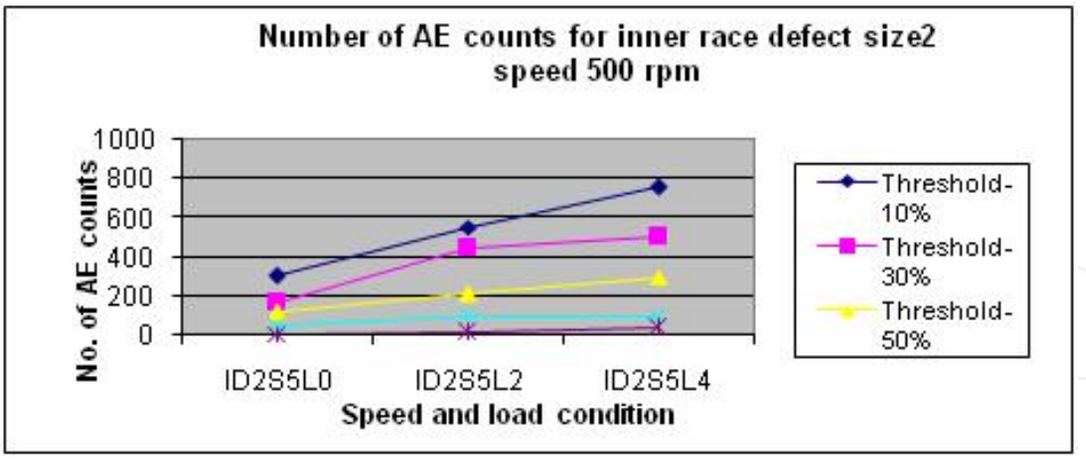

Figure 28. Number of AE counts for inner race defect size2 at speed 500 rpm

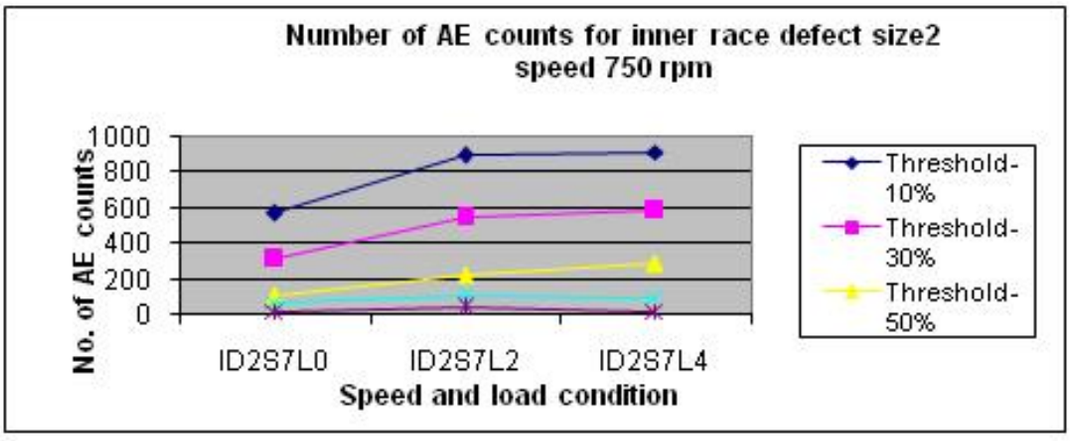

Figure 29. Number of AE counts for inner race defect size2 at speed 750 rpm

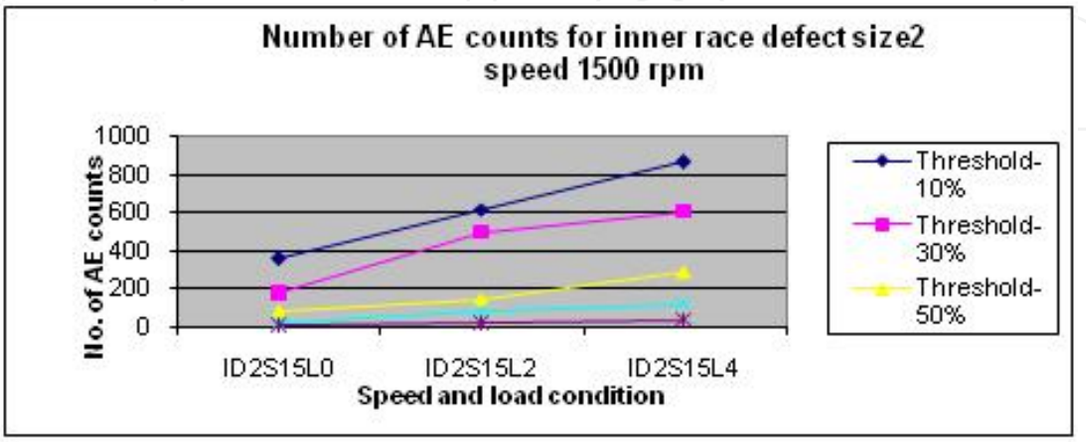

Figure 30. Number of AE counts for inner race defect size2 at speed 1500 rpm

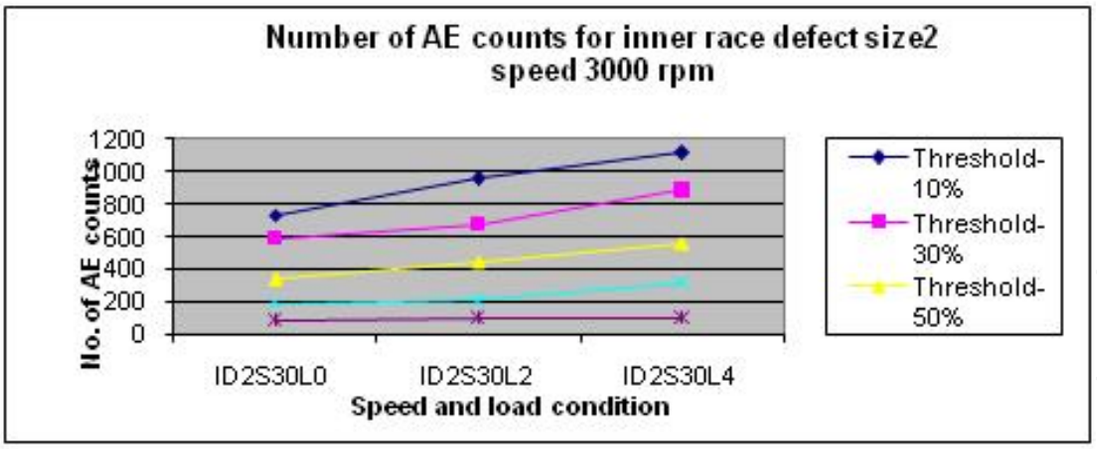

Figure 31. Number of AE counts for inner race defect size2 at speed 3000 rpm

For inner race defect size 2, at 300 rpm the AE counts increases as load increases at threshold levels of 30% and 10%. Whilst at 500 rpm and 750 rpm the AE counts increases as load increases at threshold levels of 50%, 30%, and 10%. And at 1500 rpm and 3000 rpm the AE counts increases as load increases at 70%, 50%, 30%, and 10% threshold levels. It is difficult to distinguish the AE counts of defect size 1 with defect size 2 for all respective speeds and threshold levels.

10. Conclusion

The results of the study shows AE counts can be used to detect defects in bearings. It also shows the correlation between the AE counts with speeds and loads. It is important to choose the appropriate range of threshold levels. A range of at least 30% (90%, 70%, 50%, 30%) of the maximum amplitude of the background noise was found to be effective..Morhain and Mba [4] stated that there isn't an ideal threshold level for all operating condition in bearing diagnosis, so investigation of background noise at all operational speed can be very useful. The use of AE r.m.s and counts is more successful for ball defects rather than inner race defects..

Author details

Zahari Taha[1] and Indro Pranoto[2]

1 Faculty of Mechanical Engineering, University Malaysia Pahang, Malaysia

2 Department of Mechanical and Industrial Engineering, Gadjah Mada University, Indonesia

http://dx.doi.org/10.5772/55434

References

[1] Roger LM, The application of vibration signature analysis and acoustic emission source location to on-line monitoring of antifriction bearing, Tribology International 12(2) (1979): 51-9

[2] Yoshioka T, Fujiwara T, New acoustic emission source locating system for the study of rolling contact fatigue, Wear 81(1) (1982):183-6

[3] Yoshioka T, Fujiwara T, Application of acoustic emission technique to detection of rolling bearing failure, American Society of Mechanical Engineers 14(1984): 55-76

[4] Morhain A, Mba D, Bearing defect diagnosis and acoustic emission, Journal of Engineering Tribology, Institution of Mechanical Engineering 217(4) (Part J) (2003) 257-272 (ISSN 1350-6501)

[5] Smith JD, Vibration monitoring of bearings at low speeds, Tribology International 1982; June: 139-44

[6] McFadden PD, Smith JD, Acoustic emission transducer for the vibration monitoring of bearings at low speeds, Proc. IMechE 198(C8) (1984):127-30

[7] Tandon N, Nakra BC, Defect detection in rolling element bearings by acoustic emission method, J Acoustic Emission 9(1) (1990): 25-8

[8] Tan CC, Application of acoustic emission to the detection of bearing failures, In: Proceeding, Tribology Conference, Brisbane, Australia: Institution of Engineers, 1990:110-4

[9] Bansal V, Gupta BC, Prakash A, Eshwar VA, Quality inspection of rolling element bearing using acoustic emission technique, J Acoustic Emission 9(2)(1990):142-6

[10] Hawman M.W., Galinaitis W.S., Acoustic emission monitoring of rolling element bearings, Proceedings of the IEEE, Ultrasonics Symposium (1988): 885-9

[11] Choudhury A, Tandon N, Application of acoustic emission technique for detection of defects in rolling element bearings, Tribology International 33 (2000): 39-45

[12] Abdullah M.A., David Mba, A comparative experimental study on the use of acoustic emission vibration analysis for bearing defect identification and estimation of defect size, Mech. System and Signal Processing J (2004): 1-35

[13] C. James Li, S.Y. Li, Acoustic emission analysis for bearing condition monitoring, Wear 185 (1995): 67- 74

[14] E. Downharm and R. Wood, The rationale of monitoring vibration on rotating machinery in continuously operating process plant, ASME Paper No.71- vibr-96

[15] B. Wiechbrodt and J. Bowden, Instrument for predicting bearing damage, GE company Rep., March, 1970, S-70-1021 AD 869633

[16] D. Dyer and R.M. Stewart, Detection of rolling element bearing damage by statistical vibration analysis, J. Mech (1978):229-235

[17] O.G. Gustafsson and T. Tallian, Detection of damage in assembled rolling bearings, Trans. Am. Soc. Lubric. Eng., 5 (1962):197-205

[18] Tedric A. Harris, Rolling Bearing Analysis, 4th Ed., John Wiley and Sons, Inc, USA, 2001

[19] Zhang Zhen, A Tool Condition Monitoring Approach Based on SVM, Master Thesis, National University of Singapore, 2002